Title

Effect of phase homogeneity and grain size on ferroelectric properties of 0.5Ba(Zr0.2Ti0.8)O3–0.5(Ba0.7Ca0.3)TiO3 (BXT) lead-free ceramics

Authors

Dupuy, AD
Kodera, Y
Carman, GP
et al.

Publication Date

2019

DOI

10.1016/j.scriptamat.2018.08.051

Peer reviewed

Scripta Materialia 159 (2019) 13–17

Contents lists available at ScienceDirect

Scripta Materialia

journal homepage: www.elsevier.com/locate/scriptamat

Effect of phase homogeneity and grain size on ferroelectric properties of $0.5Ba(Zr_{0.2}Ti_{0.8})O_3–0.5(Ba_{0.7}Ca_{0.3})TiO_3$ (BXT) lead-free ceramics

A.D. Dupuy [a,1], Y. Kodera [a], G.P. Carman [b], J.E. Garay [a,*]

[a] Advanced Materials Processing and Synthesis Lab, Mechanical and Aerospace Engineering Department, University of California, San Diego, United States of America
[b] Mechanical and Aerospace Engineering Department, University of California, Los Angeles, United States of America

ARTICLE INFO

Article history:
Received 18 May 2018
Received in revised form 29 August 2018
Accepted 30 August 2018
Available online xxxx

Keywords:
Spark plasma sintering (SPS)
CAPAD
BZT-BCT

ABSTRACT

We used two different solid state synthesis routes in conjunction with Current Activated Pressure Assisted Densification (CAPAD) to produce lead-free $0.5Ba(Zr_{0.2}Ti_{0.8})O_3–0.5(Ba_{0.7}Ca_{0.3})TiO_3$ (called BZT-BCT or BXT) ceramics. The materials are fully dense and have a wide range of grain sizes from nanocrystalline (90 nm) to more conventional micrometer size range (3 μm). We investigate the role of grain size and phase homogeneity on the dielectric and ferroelectric properties of BXT independent of porosity. One of the synthesis routes yields samples with comparably high switchable polarization, $2P_r$ at grain sizes ~7 times smaller (420 nm) than the former route.

Since the first report in 2009, $0.5Ba(Zr_{0.2}Ti_{0.8})O_3–0.5(Ba_{0.7}Ca_{0.3})TiO_3$ (called BZT-BCT or BXT) has emerged as one of the most promising lead free ferroelectric materials [1]. A substantial amount of work has been devoted to understanding the origin of the ferroelectric behavior of BXT [2], leading to important insights of the underlying ferroelectric mechanisms. Briefly, the performance is primarily attributed to the mixed Orthorhombic and Tetragonal phase states [3]. Having access to these distinct phases [4] yields some unique ferroelectric phenomena, such as a temporary single domain states [5] and nanodomains [6]. Together, these phenomena contribute to the exceptional properties of BXT.

Little work however, has been done on the influence of microstructure on the properties of BXT. Most studies have used traditional free-sintering to densify BXT ceramics which has produced a relatively narrow range of microstructures. More flexible methods are needed to explore a wider range of grain sizes and phase homogeneity. Current Activated Pressure Assisted Densification (CAPAD) (often called spark plasma sintering (SPS)) [7] has emerged as an ideal tool for isolating specific microstructural features [8]. Various ferroelectric materials have been successfully densified using CAPAD [9]. Previous studies have used several different densification methods (including CAPAD) to examine a wide range of grain sizes (0.4–32.2 μm) [10,11]. However, these studies produced samples with varying porosity. Thus, the true influence of grain size on the ferroelectric properties of BXT has yet to determined.

Powder characteristics often dictate achievable microstructures. BXT powders are most commonly synthesized using a solid-state reaction involving a large quantity (~56 wt%) of $BaCO_3$. Calcination temperatures of 1300 °C for several hours are typically required to completely decompose the carbonates, leading to grain growth and agglomeration. Other synthesis techniques, such as sol-gel [12,13] and auto combustion methods [14] have been used as well. These methods produce high quality BXT powders, but they lack the simplicity of solid-state methods. Additionally, previous work on BXT ceramics does not rigorously verify the completeness of the reaction. Phase purity is typically examined using only XRD, which is insufficient for determining inhomogeneity.

Previously we demonstrated optical transparency and remarkable electro-optic properties in BXT by using a new powder synthesis route and CAPAD [15]. The primary innovation of the synthesis was replacing $BaCO_3$ with $BaTiO_3$ as the principal source of Ba. This method requires lower temperatures to form BXT, resulting in ceramics with finer grain sizes and homogenous phase distributions. As it relies primarily on $BaTiO_3$, this synthesis method is referred to as the BT method. The conventional method will be referred to as the BC-based method due to its reliance on $BaCO_3$.

In this work, we leverage the two synthesis routes to demonstrate the influence of microstructure (grain size and phase homogeneity) on the ferroelectric and dielectric properties of BXT. Ceramics synthesized from both BC and BT based powders are processed to full density using the CAPAD and the effect of processing temperature and powder synthesis method on the microstructure are explored. In addition, we examine the influence of grain size and phase homogeneity on the ferroelectric properties of BXT independent of the effects of porosity.

Solid-state synthesis methods were used for the preparation of BXT powders. Both synthesis routes involved first using a mortar and pestle

* Corresponding author.
E-mail address: jegaray@ucsd.edu (J.E. Garay).
[1] Current address: Chemical Engineering and Materials Science Department, University of California, Irvine, United States of America.

https://doi.org/10.1016/j.scriptamat.2018.08.051
1359-6462/

to hand mix components followed by tumble ball milling for 6 h in ethanol. BC-based powders were prepared using $BaCO_3$ (99.9% MTI Corp., Richmond, CA, USA), $BaZrO_3$ (99% Alfa Aesar, Ward Hill, MA, USA), $CaCO_3$ (98% Reade Advanced Materials, Reno, NV, USA), and TiO_2 (99.9% Alfa Aesar). BT-based BXT powders were prepared using $BaTiO_3$ (99.95% Inframat Advanced Materials, Manchester, CT, USA), ZrO_2 (ppm impurity, Tosoh Corporation, Tokyo, Japan), $CaCO_3$ (98% Reade Advanced Materials), and TiO_2 (99.99% MTI Corp). TGA analysis (not shown) along with trial and error was used to determine the minimum necessary calcination conditions for complete elimination of carbonate content. These conditions were found to be 18 h at 1000 °C for BC-based powders and 1 h at 850 °C for BT-based powders.

Calcined BT and BC-based BXT powders were densified using a custom built CAPAD device [16]. BC-based powders were densified at 1200, 1250, and 1300 °C, measured using an optical pyrometer. BT based powders were densified at 1000, 1050, 1100, and 1200 °C, measured using an N-type thermocouple. All BXT samples were held at temperature for 5 min under 100 MPa of pressure. A heating rate of 200 °C/min and a cooling rate of 50 °C/min were used.

The densities of the samples were measured using the Archimedes method and relative density was calculated using 5.789 g/cm^3 as the theoretical density [17]. Densified samples were heat treated in air at 750 °C for 12 h to eliminate oxygen vacancies created from the reducing atmosphere in the CAPAD. Samples were then polished down to 1 μm diamond slurry. Microstructural analysis was performed using a XL-30 Scanning Electron Microscope (Philips, The Netherlands) and a Zeiss Sigma 500 (Carl Zeiss, Germany). Grain size of BC based ceramics was assessed from polished surfaces etched with HCl. SEM of fracture surfaces were used to determine the average grain size of BT based ceramics, by measuring >500 grains on random sample locations on multiple micrographs. Phase homogeneity was examined on polished surfaces using the SEM in backscatter electron (BSE) mode. Focused Ion Beam (FIB) milling from a FEI Quanta™ 3D 200i (FEI, OR) was used to further polish a BT based sample densified at 1000 °C for the purposes of examining its phase homogeneity using BSE. Densified samples and powders were analyzed with XRD using a PANalytical Empyrean (PANalytical, The Netherlands).

Dielectric and ferroelectric measurements were performed at room temperature on cylindrical samples prepared in the parallel plate capacitor style with silver paste applied to the faces. Permittivity was measured using an HP4284A LCR meter (Agilent, CA) with a 1 kHz frequency. Ferroelectric hysteresis loops were acquired using a custom built Sawyer-Tower measurement device with a virtual ground design. Voltage was applied using a Trek 610E high voltage amplifier (Trek Inc., USA). To ensure consistent initial conditions, samples were poled at room temperature with 2.3 MV/m for 1 h before measuring. The power supply was driven by a Rigol DG4062 function generator (Rigol Technologies Inc., China). Hysteresis loops were acquired at a maximum field of 3 MV/m at a driving frequency of 60 mHz.

Table 1 summarizes the microstructural and electronic properties of the densified ceramics. All the samples have >99% relative densities so that porosity does not significantly contribute to the properties. Fig. 1a and b are SEM micrographs of a fracture surface of a BT-based ceramic produced at 1000 °C (finest grain sample) (1a) and a polished and etched surface of a BC-based BXT produced at 1300 °C (1b). Comparison of the micrographs reveals the substantial grain size difference. The darker regions of the BT-based BXT are not pores (Archimedes measurements confirm full density) but are grain pull-outs resulting from the fracture process. To further corroborate the density measurements, we

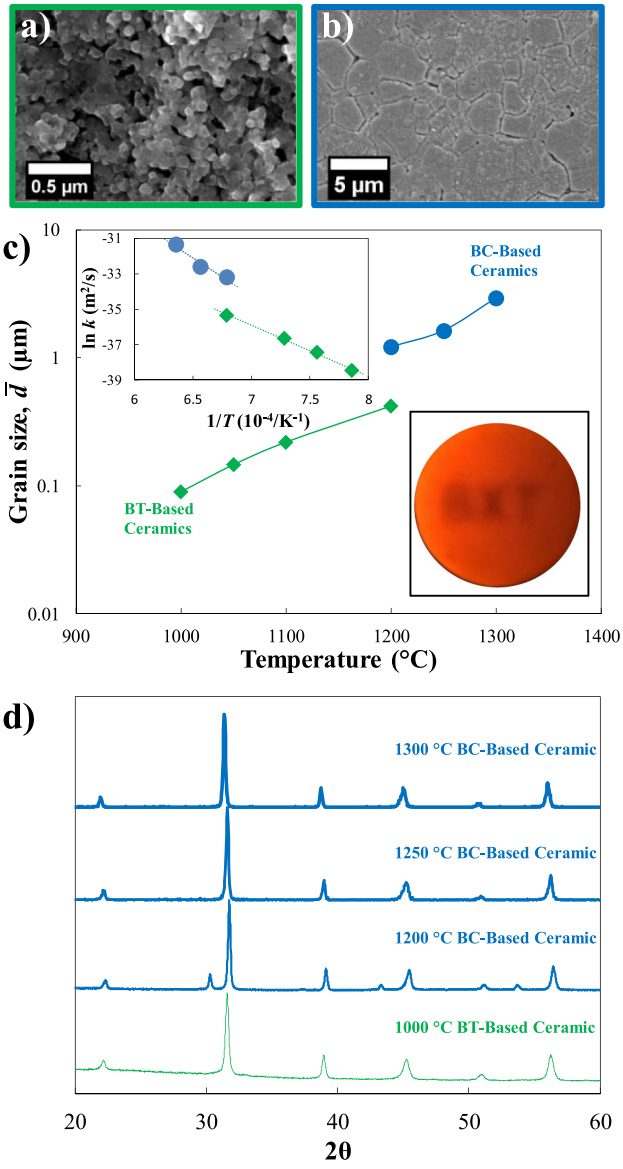

Fig. 1. Role of synthesis and processing conditions on microstructure: micrographs of the 1000 °C BT based (a) and 1300 °C BC based (b) densified ceramics. (c) Grain size and (d) XRD patterns for BXT ceramics made from both BC and BT based synthesis methods and densified at the specified CAPAD processing temperatures. The upper left inset of (c) shows the logarithmic grain growth rate k vs inverse CAPAD processing temperature. The lower right inset of (c) shows a backlit photograph of the 1000 °C BT based ceramic sitting on text. The text is legible through the translucent sample, indicating high density.

Table 1
Summary of the microstructural and electronic properties of the densified BXT ceramics processed using different CAPAD temperatures.

Synthesis method	Temperature (°C)	Phase pure?	Grain size (μm)	Density (%)	ε	$+P_r/-P_r$ (μC/m^2)	$+E_c/-E_c$ (MV/m)
BC based	1200	No	1.22 ± 0.54	99	1805	+1.05/−0.32	+0.06/−0.33
	1250	No	1.63 ± 0.67	99	2348	+1.13/−0.33	+0.06/−0.23
	1300	Yes	2.93 ± 1.23	99	3113	+1.53/1.74	+0.19/−0.17
BT based	1000	Yes	0.09 ± 0.02	99	698	+0.10/−0.10	+0.14/−0.14
	1050	Yes	0.15 ± 0.05	99	966	+0.16/−0.16	+0.14/−0.15
	1100	Yes	0.22 ± 0.09	99	1323	+0.20/−0.20	+0.16/−0.18
	1200	Yes	0.42 ± 0.18	99	1843	+1.71/−1.65	+0.30/−0.33

include a photograph of the 90 nm sample (inset in Fig. 1c) demonstrating its translucency; A high relative density is required for light transmission in ceramics [15,18].

Fig. 1c shows the role of CAPAD temperature on average grain size, $\bar{d}$ for the densified BXT samples. BC-based samples exhibit significantly larger grain sizes overall than the BT-based samples due to the higher calcining temperature required for BC-based synthesis. SEM (not shown here) of both powders show that the BC-based powders are dominated by relatively large agglomerates ranging in size from 0.5 to 1.5 μm. The agglomeration in the powders will contribute to the large grain sizes in the BC-based ceramics. By contrast, the BT-based powders are primarily agglomerate free, displaying only occasional <0.5 μm sized agglomerates. The largest $\bar{d}$ achieved was 2.93 μm produced from BC powders densified at 1300 °C while the smallest $\bar{d}$ was 90 nm from BT-based powders densified at 1000 °C.

A 90 nm grain size in the densified ceramics is less than double the reported grain size of the $BaTiO_3$ powder, the primary constituent in BT-based synthesis (~86 wt%). We attribute this small grain growth to the low calcining and CAPAD temperatures allowed by the BT-based process. These results are in-line with previous results by Mukherjee and co-workers showing that $BaTiO_3$ is resistant to grain growth at similar temperatures [19].

Since all samples are fully dense, we used grain size measurements to analyze grain growth kinetics. Normal grain growth kinetics can be described using $\bar{d}^2 - d_o^2 = kt$ where $\bar{d}$ is the average grain size, d_o is the initial average grain size (at $t = 0$), k is the grain growth rate which is related to grain boundary mobility, M, the grain boundary energy, γ and a geometric constant α which is often approximated as 1 such that $k = 2\alpha\gamma M$. k is expected to have an Arrhenius temperature, T dependence, $k(T) = k_o \exp(-E_{gg}/RT)$ where E_{gg} is the activation energy for grain growth, k_o is a frequency factor and R is the gas constant. Although it is typical to find $k(T)$ using multiple hold times at each temperature, here we measure k for the hold time of 5 min at each temperature. We believe that the high heating and cooling rates make this a good approximation. The results are plotted in the inset of Fig. 1c. The dashed lines are linear fits; the excellent agreement for both the BC ($R^2 = 0.948$) and BT ($R^2 = 0.996$), reveal that grain growth at these temperatures is normal diffusion (grain boundary migration) controlled growth. This is in contrast to grain growth studies in other perovskites (strontium titanate and barium titanate) that have reported anomalous grain growth likely due to grain boundary structure transitions at higher temperatures, $T < 1350$ °C [20,21]. This stresses the importance of using low densification temperatures to avoid abnormal grain growth.

XRD patterns for densified ceramics processed at different CAPAD temperatures can be seen in Fig. 1d. All patterns show the familiar perovskite structure as the major constituent. The BC-based sample processed at 1200 °C shows peaks corresponding to unreacted $BaZrO_3$. Remarkably, the BT-based sample densified at 200 °C lower temperature (1000 °C) does not show extraneous peaks. The remaining two (1250, 1300 °C) BC patterns also do not show any extraneous peaks, implying phase homogeneity.

SE and BSE micrographs can provide additional insight into the phase homogeneity of the densified BC based samples (Fig. 2a). As expected from the XRD, the BC-based sample densified at 1200 °C show visible inhomogeneity. In addition, the 1250 °C sample also displays a small amount of inhomogeneity which is not indicated in the XRD patterns, showing that XRD is insufficient for determining phase purity.

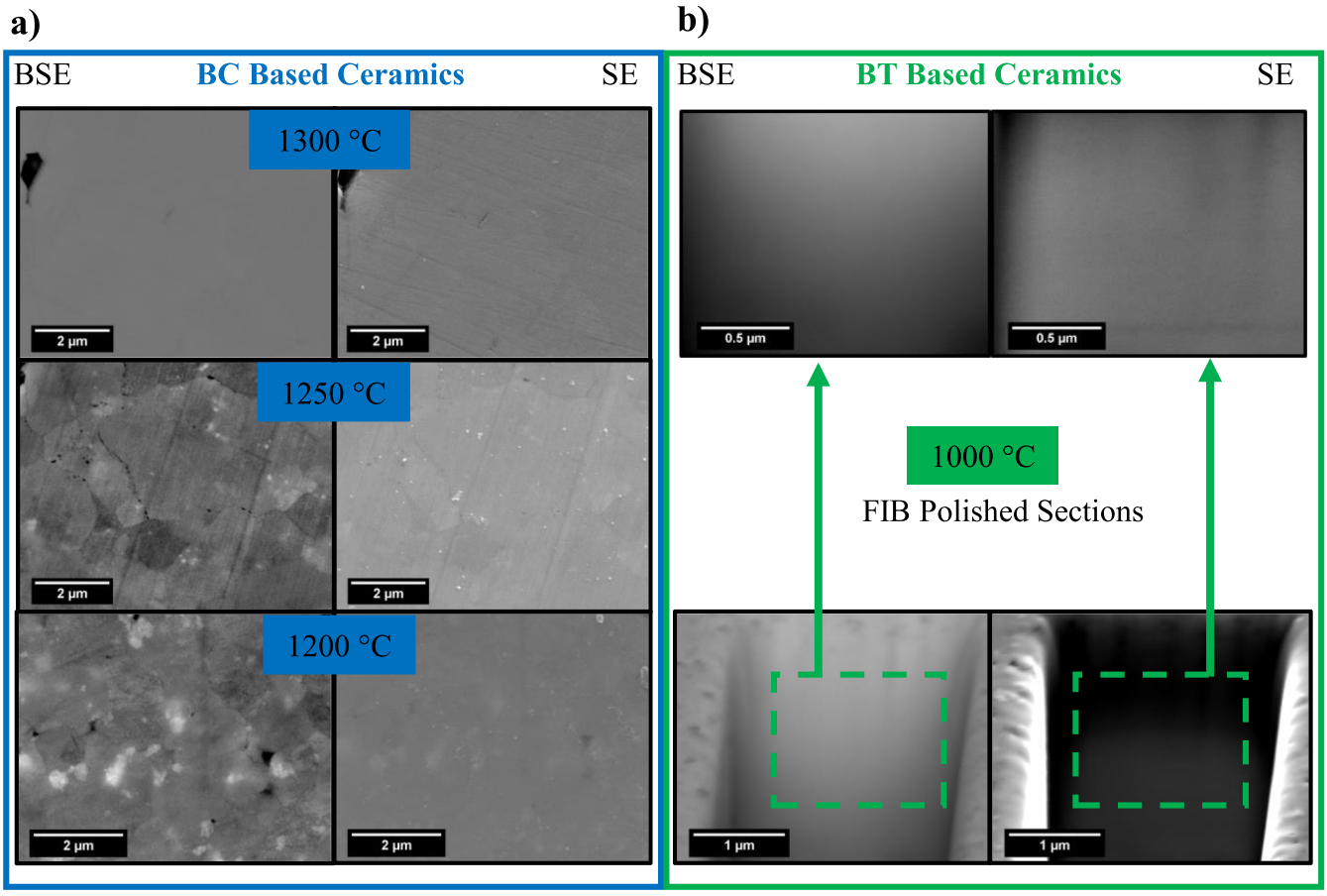

Fig. 2. Analysis of phase homogeneity: SE and BSE micrographs of the BXT ceramics produced from different synthesis and CAPAD processing temperatures. (a) BC based synthesis and 1200 °C, 1250 °C, and 1300 °C CAPAD densification. (b) BT based synthesis and 1000 °C CAPAD densification. Higher magnification micrographs are provided to demonstrate the fine scale of the phase homogeneity.

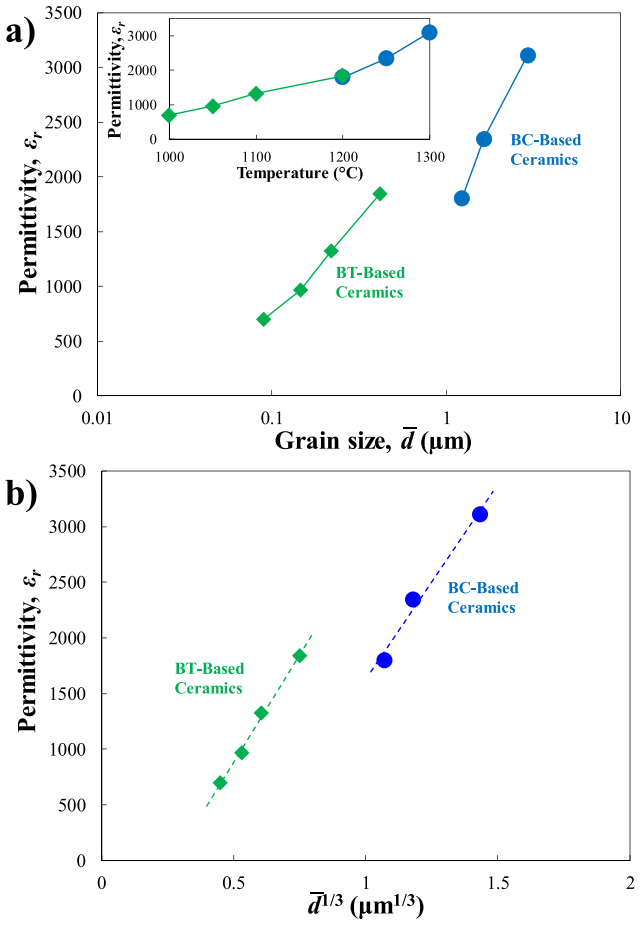

Fig. 3. Role of microstructure on dielectric properties: (a) Permittivity versus average grain size $\bar{d}$ for densified ceramics from both BC and BT powder synthesis methods. The inset shows permittivity vs CAPAD processing temperature for those same ceramics. (b) Permittivity versus $\bar{d}^{1/3}$ for those same densified ceramics.

Samples densified at 1300 °C show no sign of inhomogeneity. In stark contrast to the BC-based ceramics, SE and BSE micrographs of a BT-based BXT densified at 1000 °C show full phase homogeneity (Fig. 2b). These micrographs were taken on FIB-polished sections to confirm homogeneity down to nanometric length scales. BT-based synthesis combined with CAPAD processing produces fully dense phase pure BXT at temperatures as low as 1000 °C; 300 °C lower than required for BC-based samples using CAPAD and 500 °C lower than the commonly used free-sintering temperatures (1500 °C) [1].

Fig. 3a introduces the $\bar{d}$ dependence of permittivity, ε_r for densified ceramics; ε_r increases with $\bar{d}$ and processing temperature (inset). The ε_r of polycrystalline ceramics is known to decrease in samples with very fine grains. This scaling effect (decrease) at fine grain sizes is attributed to a number of different phenomena such as dilution by the grain boundaries (gbs), reduction of the density and/or mobility of domain boundaries, pinning of domains at interfaces [22,23], and interference from space charge layers [24]. A common argument is that the permittivity of the gb regions is significantly lower than the bulk and since the relative fraction of gbs scales with $d^{1/3}$, one expects an $\varepsilon_r \propto d^{1/3}$ behavior. The measured permittivity of the BC-Based and BT-based samples is plotted as a function of $d^{1/3}$, in Fig. 3b; The excellent fit (R^2 = 0.996 for BT-based and 0.983 for BC-based) is in-line with dilution caused by gbs.

The highest permittivity (ε_r = 3113 at 2.9 μm) was achieved at 1300 °C with the BC-based synthesis. This permittivity is very similar to what was found in the original BXT (ε_r = 3060) by free-sintering at 1500 °C [1]. A more surprising result is that the BT-based sample produced at 1200 °C has a similar permittivity (ε_r = 1843) compared to the 1200 °C BC-based sample (ε_r = 1805) despite the large $\bar{d}$ difference (0.42 μm vs. 1.2 μm). Since all the samples are fully dense, this more aggressive decline in permittivity can be attributed to phase inhomogeneity.

Ferroelectric hysteresis of the BC-based ceramics is shown in Fig. 4a. A symmetric slim loop is achieved in the ceramic densified at 1300 °C. By contrast, the ceramics densified at 1250 and 1200 °C produce even slimmer hysteresis loops with a small shift along electric field axis (*i.e.*, loops are not symmetric about $E = 0$). In addition, a noticeable distortion under negative fields can be observed in the hysteresis loop of the 1200 °C ceramic. The inset in Fig. 4a shows the magnification of the second quadrant. Decreasing the CAPAD processing temperature results in an increasingly distorted hysteresis loop and a decrease in the remnant polarization, P_r in the BC-based ceramics.

Like the decrease in permittivity, we believe this decrease in P_r can be attributed to inhomogeneity in the lower temperature samples. Wang et al. suggested [25] that inhomogeneity in ferroelectric materials decreases their properties due to a "dilution" by a phase with worse/no ferroelectric properties. This effect is compounded in multiphase ferroelectric materials (such as BXT) due to the inhomogeneities producing local regions with compositions not in the phase boundaries, resulting in even lower properties. This dilution effect will certainly exist in the inhomogeneous samples since BXT properties should be maximized at the phase boundary [1] and the extraneous phase ($BaZrO_3$) is paraelectric.

The distortions in the hysteresis for the inhomogeneous ceramic (1200 °C) in Fig. 4a, indicate effects in addition to dilution. Asymmetry and distortions in a hysteresis loop are commonly attributed to the presence of charged point defects pinning domains and inhibiting domain motion [23,26]. Higher distortion is commonly observed in ferroelectric ceramics that are purposely doped to achieve a "hardening" effect [27–29]. It is possible that the inhomogeneous BC-Based samples exhibit unintentional hardening effect from point defects that arise from incomplete reaction.

Fig. 4b shows the measured *P-E* loops for the BT-based ceramics. CAPAD at 1200 °C produces a familiar ferroelectric hysteresis response. The polarization response changes dramatically, however, in the ceramics processed at 1100 °C and below that reveal an apparent loss of ferroelectric behavior.

The loss of hysteresis at very fine grain sizes has been observed in other ferroelectric materials as well [30, 31]. It is believed that this is due to the dominance of the above mentioned scaling phenomena, causing the electric fields required for domain switching to exceed the breakdown field of the material [32]. The increase in gb concentration will lead to a reduced ferroelectric response for two reasons. The gbs themselves will have a mostly linear polarization response to electric field, resulting in a dilution of the ferroelectric response in our nanoceramics. Additionally, a high concentration of gbs leads to an inhomogeneous local electric field, reducing the effective field on the grain core [33]. Since our BT-based ceramics are fully dense and phase pure, this reduction in ferroelectric and dielectric properties can be attributed solely to grain size.

The grain size dependence of the ferroelectric properties are summarized in Fig. 4c and d. Fig. 4c plots the switchable polarization, $2P_r = P_r^+ + |P_r^-|$ where P_r^+ and P_r^- is the positive and negative remnant polarization vs. grain size. Although the BT based samples processed at <1100 °C are not meaningfully ferroelectric, the P_r and E_c values for these ceramics are given in order to compare with other samples. They are determined by the point where the polarization loop crosses the y-axis and x-axis respectively. The switchable polarization increases with $\bar{d}$ for both samples sets, however, the $2P_r$ of the BT-based sample is as high as the highest BC-based sample although it has ~7× smaller $\bar{d}$ (0.42 μm compared to 2.93 μm). Figs. 4d plots the internal bias field, $E_{ib} = (E_c^+ + E_c^-)/2$ where E_c^+ and E_c^- are the positive and negative coercivities respectively. The data shows that all the

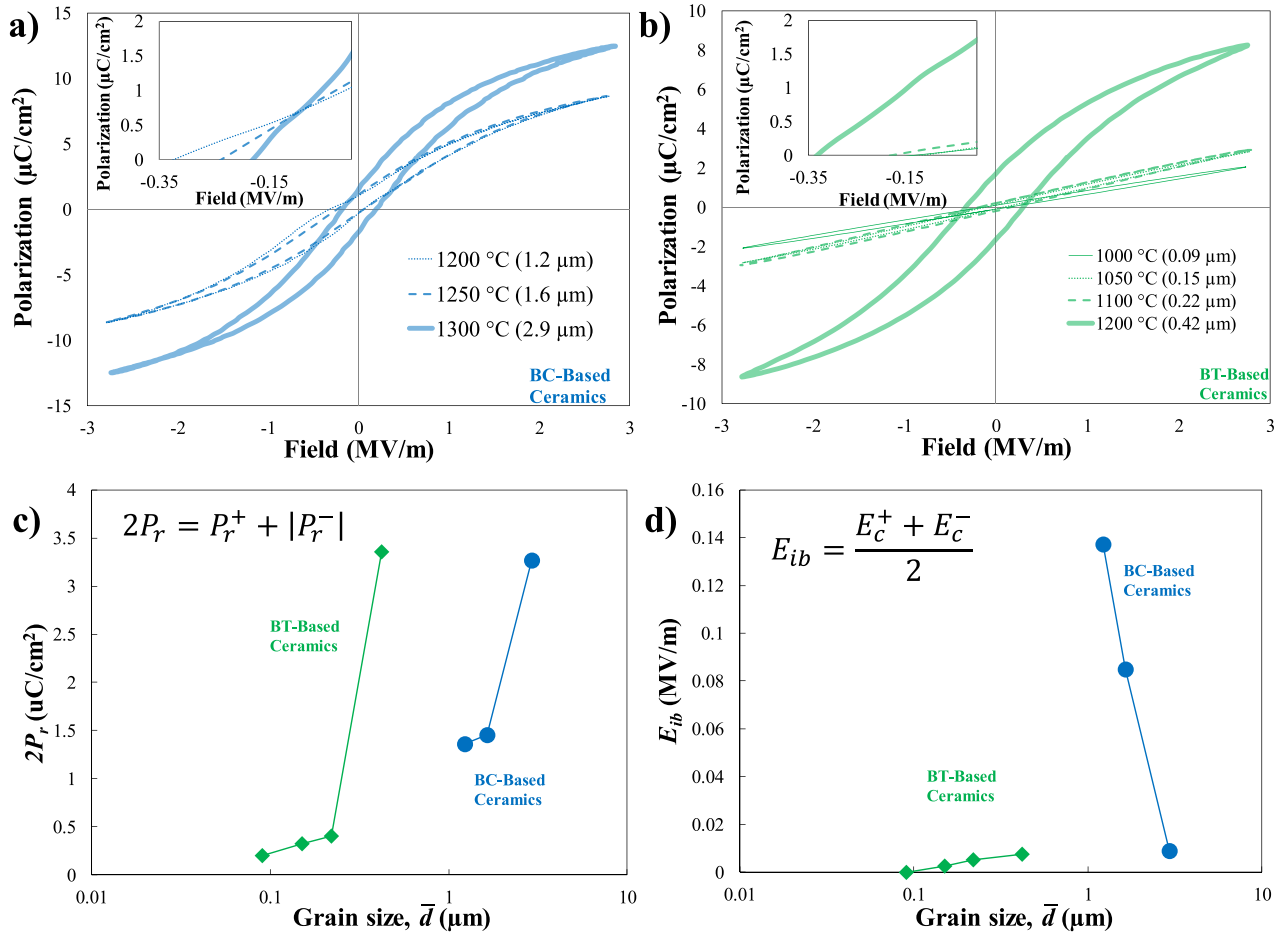

Fig. 4. Role of microstructure on ferroelectric properties: (a) P-E ferroelectric hysteresis loop for the BC based densified ceramics. The inset displays the second quadrant in more detail. (b) P-E ferroelectric hysteresis loop for the BT based densified ceramics. The inset displays the second quadrant in more detail. (c) Switchable polarization $2P_r$ and (d) internal bias field E_{ib} for the BC and BT based densified ceramics.

BT-based samples have minimal E_{ib} while the BC-based samples decrease within increasing processing temperature likely due to increased sample homogeneity.

Acknowledgements

We thank Mr. J. Cortez and Mr. D. Cataldi for help with sample preparation. Funding of this work by the NSF through Award # 0956071 with Dr. L. Madsen as program director is most gratefully acknowledged.

References

[1] W. Liu, X. Ren, Phys. Rev. Lett. 103 (2009) 1.
[2] M. Acosta, N. Novak, V. Rojas, S. Patel, R. Vaish, J. Koruza, G.A. Rossetti, J. Rödel, Appl. Phys. Rev. 4 (2017), 041305.
[3] D.S. Keeble, F. Benabdallah, P.A. Thomas, M. Maglione, J. Kreisel, Appl. Phys. Lett. 102 (2013), 092903.
[4] M. Acosta, N. Khakpash, T. Someya, N. Novak, W. Jo, H. Nagata, G.A. Rossetti, J. Rödel, Phys. Rev. B 91 (2015), 104108.
[5] H. Guo, C. Zhou, X. Ren, X. Tan, Phys. Rev. B 89 (2014) 100104.
[6] M. Zakhozheva, L.A. Schmitt, M. Acosta, W. Jo, J. Rödel, H.-J. Kleebe, Appl. Phys. Lett. 105 (2014), 112904.
[7] J.E. Garay, Annu. Rev. Mater. Res. 40 (2010) 445.
[8] F. Maglia, I.G. Tredici, U. Anselmi-Tamburini, J. Eur. Ceram. Soc. 33 (2013) 1045.
[9] T. Hungría, J. Galy, A. Castro, Adv. Eng. Mater. 11 (2009) 615.
[10] J. Hao, W. Bai, W. Li, J. Zhai, J. Am. Ceram. Soc. 95 (2012) 1998.
[11] F. Benabdallah, C. Elissalde, U.-C.C. Seu, D. Michau, A. Poulon-Quintin, M. Gayot, P. Garreta, H. Khemakhem, M. Maglione, J. Eur. Ceram. Soc. 35 (2015) 4153.
[12] J. Paul Praveen, K. Kumar, A.R. James, T. Karthik, S. Asthana, D. Das, Curr. Appl. Phys. 14 (2014) 396.
[13] V.S. Puli, A. Kumar, D.B. Chrisey, M. Tomozawa, J.F. Scott, R.S. Katiyar, J. Phys. D. Appl. Phys. 44 (2011), 395403.
[14] G.K. Sahoo, R. Mazumder, J. Mater. Sci. Mater. Electron. 25 (2014) 3515.
[15] A.D. Dupuy, Y. Kodera, J.E. Garay, Adv. Mater. 28 (2016) 7970.
[16] S.R. Casolco, J. Xu, J.E. Garay, Scr. Mater. 58 (2008) 516.
[17] J.P. Praveen, T. Karthik, A.R. James, E. Chandrakala, S. Asthana, D. Das, J. Eur. Ceram. Soc. 35 (2015) 1785.
[18] Y. Kodera, C.L. Hardin, J.E. Garay, Scr. Mater. 69 (2013) 149.
[19] J. Liu, Z. Shen, W. Yao, Y. Zhao, A.K. Mukherjee, Nanotechnology 21 (2010) 75706.
[20] J.G. Fisher, S.-Y. Choi, S.-J.L. Kang, J. Am. Ceram. Soc. 89 (2006) 2206.
[21] W. Rheinheimer, M.J. Hoffmann, Curr. Opin. Solid State Mater. Sci. 20 (2016) 286.
[22] J.F. Ihlefeld, D.T. Harris, R. Keech, J.L. Jones, J.-P. Maria, S. Trolier-McKinstry, J. Am. Ceram. Soc. 99 (2016) 2537.
[23] L. Jin, F. Li, S. Zhang, J. Am. Ceram. Soc. 97 (2014) 1.
[24] K. Okazaki, K. Nagata, J. Am. Ceram. Soc. 56 (1973) 82.
[25] Y. Wang, D. Damjanovic, N. Klein, E. Hollenstein, N. Setter, J. Am. Ceram. Soc. 90 (2007) 3485.
[26] K. Carl, K.H. Hardtl, Ferroelectrics 17 (1977) 473.
[27] L. Chen, H. Fan, S. Zhang, J. Am. Ceram. Soc. 100 (2017) 3568.
[28] J.B. Lim, S. Zhang, J.-H. Jeon, T.R. Shrout, J. Am. Ceram. Soc. 93 (2010) 1218.
[29] T.M. Kamel, G. de With, J. Eur. Ceram. Soc. 28 (2008) 1827.
[30] M. Buscaglia, M. Viviani, V. Buscaglia, L. Mitoseriu, A. Testino, P. Nanni, Z. Zhao, M. Nygren, C. Harnagea, D. Piazza, C. Galassi, Phys. Rev. B 73 (2006), 064114.
[31] X.-H. Wang, I.-W. Chen, X.-Y. Deng, Y.-D. Wang, L.-T. Li, J. Adv. Ceram. 4 (2015) 1.
[32] L. Curecheriu, S.-B. Balmus, M.T. Buscaglia, V. Buscaglia, A. Ianculescu, L. Mitoseriu, J. Am. Ceram. Soc. 95 (2012) 3912.
[33] L. Padurariu, L. Curecheriu, V. Buscaglia, L. Mitoseriu, Phys. Rev. B 85 (2012), 224111.